International Journal of Heat and Mass Transfer 55 (2012) 6060–6066

Contents lists available at SciVerse ScienceDirect

International Journal of Heat and Mass Transfer

journal homepage: www.elsevier.com/locate/ijhmt

Molecular dynamics studies of ultrafast laser-induced phase and structural change in crystalline silicon

Chengjuan Yang [a,b], Yaguo Wang [b], Xianfan Xu [b,*]

[a] School of Mechanical Engineering, Xi'an Jiaotong University, Xi'an, Shaanxi Province 710049, PR China
[b] School of Mechanical Engineering, Birck Nanotechnology Center, Purdue University, West Lafayette, IN 47907, USA

ARTICLE INFO

Article history:
Received 7 November 2011
Received in revised form 26 May 2012
Accepted 4 June 2012
Available online 2 July 2012

Keywords:
Molecular dynamics simulation
Ultrafast laser
Melting
Resolidification

ABSTRACT

In this work, thermodynamic phenomena in crystalline silicon irradiated by an ultrafast laser pulse were studied using the method of molecular dynamics simulations. The Stillinger–Weber potential was used to model the crystalline silicon. The temperature development in silicon when heated by an ultrafast laser pulse was tracked. Melting and resolidification processes and the resulting structural change were investigated. Radial Distribution Functions were used to track the liquid-amorphous interface during resolidification. It was found that the temperature at the solid–liquid interface could deviate from the equilibrium melting temperature by several hundred degrees. After the melted layer was solidified, some melted material became crystalline and the rest of the material remained in an amorphous state. The difference in the final state was associated with the rate of resolidification and both of the qualitative and quantitative analyses of the relationship between the final atom structure and resolidification rate were made.

1. Introduction

Crystalline silicon is an important material widely used in electronic industry. In the last decades (the "Silicon Era") [1], it has been the most important technological material because of its availability at an affordable cost, and its essential role for the development of electronic devices on which electronic and information revolution is based. However, it is a big challenge to machine silicon with traditional tools because of its thermal and mechanical properties. Recently, the use of ultrafast laser in material processing has attracted significant interests, due to a number of advantages of ultrafast laser machining such as highly localized material removal, reduced heat-affected zone (HAZ), and minimal debris formation compared with machining using longer pulsed lasers [2–4]. In order to obtain desired processing results, it is essential to understand the microscopic mechanism controlling the laser-induced phenomena.

The interaction of ultrafast laser pulses with a target material happens at a small time scale (picosecond or less) and a small spatial scale along the laser beam irradiation direction (tens of nanometers), accompanied with strong nonlinear, non-equilibrium, optically, thermally, and mechanically coupled processes. Research on ultrafast laser interactions with silicon has been started several decades ago with respect to laser-induced phase transitions [5,6] as well as the fundamental processes during laser ablation [7,8]. For numerical modeling, the traditional continuum approach to explore heat transfer and thermal mechanical coupling becomes questionable due to the extreme heating and non-equilibrium states obtained during the process [9]. On the other hand, Molecular Dynamics (MD) simulation does not need macroscopic material properties as a *priori*. It analyzes physical processes at the molecular or atomic scale, and the motion of each molecule or atom at a very small time scale can be traced and captured. Therefore, MD has the potential in the investigation of the mechanism underlying the thermal and thermomechanical phenomena during ultrafast laser-materials interactions [10–13]. Interactions between ultrafast laser pulses and silicon have been simulated using a molecular dynamics model and a 1-D heat diffusion model in which Langevin dynamics was used to couple the two methods [14]. The threshold fluences for material's removal were estimated and the results were comparable to experimental values. In addition, the microstructures resulted from laser-matter interactions are often of interest. Ultrafast laser ablation and recrystallization of silicon were also studied using MD simulations [15]. It was found that the ablation occurs on a picosecond time scale and recrystallization of melted silicon leads to irregular crystalline structures around the ablated hole. A correlation between the laser parameters and resulting crystal structure during laser interactions with silicon was obtained using a combined MD/FD (finite difference) simula-

* Corresponding author. Address: 585 Purdue Mall, School of Mechanical Engineering, Purdue University, West Lafayette, IN 47907, USA. Tel.: +1 765 494 5639; fax: +1 765 494 0539.
E-mail address: xxu@ecn.purdue.edu (X. Xu).

0017-9310/$ - see front matter © 2012 Elsevier Ltd. All rights reserved.
http://dx.doi.org/10.1016/j.ijheatmasstransfer.2012.06.018

Nomenclature

C_l	material constant
ΔE_{abs}	absorbed energy
E_k	kinetic energy
I	laser beam intensity
I_0	initial incident laser beam energy
I_{init}	initial laser beam energy when time is zero
t	time
t_0	time for peak laser intensity
t_g	laser pulse width, full width at half maximum (FWHM)
T_{eq}	equilibrium melting temperature
T_{int}	melt-solid interface temperature
ΔT	interfacial superheating/undercooling temperature
V_{int}	interface velocity
Δz	distance away from the surface irradiated by laser

Greek Symbols

δ	optical penetration depth
χ	velocity scaling factor

tion method [16]. Especially, the kinetics of melting and solidification of silicon have been investigated detailedly in the context of laser processing and explosive crystallization. Using nonequilibrium molecular-dynamics (NEMD) computer simulation techniques, the maximum crystallization velocity of SiGe alloys modeled by the Stillinger–Weber potential is found to decrease below the pure component values, in agreement with the results of explosive crystallization measurements [17]. Based on the NEMD technique and Stillinger–Weber potentials, the location of the solid–liquid interface during laser thermal processing of heavily B-doped a-Si on c-Si was determined by observing the diffusion coefficients (*via* mean-square displacement data), the three-body potential energy [18], and the fraction of solid atoms in each layer [19]. Computation of the interface temperature and regrowth velocity gives an indirect view of the congruent melting temperature of these heavily boron-doped Si that is inaccessible experimentally [20]. Using the first atomic-scale computer simulation of explosive crystallization, it is found that the crystal–liquid interface temperature of amorphous material (Si or Ge) is controlled by the crystal-side heat bath, while their liquid-amorphous interface temperature is independent of the amorphous-side heat bath temperature [21]. The dependence of different crystalline morphologies of Si or Ge on different heat loss conditions was also explored [21]. Furthermore, different mechanisms for the amorphization of crystal Si were revealed that amorphization mechanism may involve a glass transition in Si [22].

Experimental studies have also been carried out to investigate ultrafast laser induced structural change. Transmission electron microscopy and scanning electron microscopy have been used to study the microstructures of femtosecond laser irradiated spots [23]. Using micro-Raman spectroscopy (μ-RS), atomic force microscopy, and laser scanning microscopy, the thickness of the amorphous layer is determined to be of the order of several tens of nanometers at fluences up to two times above the melting threshold [24]. Residual stress and amorphization of the silicon single crystal were studied using micro-Raman spectroscopy as a function of the fluence and pulse duration of the incident laser. Femtosecond laser irradiation was found to induce significant stress and amorphization in single crystal silicon. Also, effects of the laser polarization on residual stress and amorphization during femtosecond laser machining of silicon wafers were also observed [25].

The aim of this work is to use MD simulations to investigate ultrafast laser-induced phase and structural change occurring in ultrafast laser interactions with crystalline silicon. The crystalline silicon is modeled using the Stillinger–Weber potential. The temperature evolution during ultrafast laser heating, melting and resolidification processes is tracked. One focus is to understand the interface kinetics, the relation between the melting/resolidification velocity and the interface superheating and undercooling, during which the RDF was tried to be applied in determining the interface positions of crystalline-liquid and liquid-amorphous silicon; and the second focus is to understand the resulting microstructure, i.e., crystalline vs. amorphous, and the qualitative and quantitative relations between the transient process parameters and the resulting structure were fully studied.

2. Molecular dynamics simulation

In this study, crystalline silicon with an initial temperature of 300 K is irradiated by an ultrafast laser pulse. In the MD model, the movement of each atom is governed by the Newtonian equation, the force between two atoms is obtained from the corresponding potential energy that governs the interactions among atoms [26].

Many efforts have been made to find out a reliable empirical potential for crystalline silicon. Each of the potentials has significant differences in at least one aspect, yet the best choice of the potential for corresponding study is based on the consistency of what the potential can do and what the potential is needed to do [21]. The Stillinger–Weber [27–29] potential, which was parameterized by considering liquid-phase properties of silicon and gives similar diffusivities in the liquid and tendency to cluster [20], is employed in this work. In addition, the solidification process described by the Stillinger–Weber model, such as the relationships among solidification velocity, temperature, and time, is better behaved than those obtained from the embedded atom method [30] (EAM) and LJ [31,32] potentials. The large system size gives much better statistics but does not change the overall conclusions [17]. Both two-body and three-body interactions in Stillinger–Weber potential are utilized to stabilize the diamond cubic structure of crystalline silicon. The Stillinger–Weber potential is by far the most widely used for modeling silicon [33]. And the values of the adjustable parameters which reproduce the properties of crystalline, amorphous, and liquid silicon could be found in ref. [28] and [29].

The modified velocity Verlet algorithm was applied to integrate Newton's equation [34,35]. MPI has been implemented to speed up the calculation. To prepare equilibrium samples at 300 K, MD is conducted in a canonical NVT ensemble for 50 ps to stabilize the temperature and then switched to microcanonical NVE ensemble for another 50 ps. Velocity scaling is used. The final temperature we got is 298.8 K, which is very close to the desired temperature of 300 K. For all the cases studied in this paper, the periodic boundary conditions are applied along x and y directions, while the free boundary condition is used along z direction.

When silicon is exposed to intensive laser field, electrons will first absorb photons and be excited from the valence band to the conduction band. Then the hot electrons will relax and combine with holes and transfer energy to the lattice atoms. However, the electronic process is beyond the scope of classical MD simulations. In this work, the transfer of electron energy to the lattice is handled by considering a longer laser pulse. The laser pulse has a pulse

duration of t_g (centered at time t_0), which is taken as 3 ps. This t_g can be either the actual Gaussian pulse duration, or the time needed for electrons to transfer the absorbed energy to the lattice for a sub-ps laser pulse. The laser pulse is centered at 14 ps.

From the Beer-Lambert law, the intensity of an electromagnetic wave inside a material falls off exponentially from the surface as:

$$I(z) = I_0 \exp\left(-\frac{\Delta z}{\delta}\right) = I_{init} \exp\left[-(t-t_0)^2/t_g^2\right] \exp\left(-\frac{\Delta z}{\delta}\right) \quad (1)$$

where $I(z)$ is the laser beam intensity in the material, I_0 is the incident laser beam intensity at the sample surface. δ denotes optical penetration depth and its value is also listed in Table 1. Values of the parameters in Eq. (1) are all listed in Table 1. The laser energy absorbed by the material is changed to the kinetic energy of atoms, which is realized through the scaling the velocities with factor χ, expressed as:

$$\chi = \left(1 + \frac{\Delta E_{abs}}{E_k}\right)^{1/2} \quad (2)$$

where ΔE_{abs} is the absorbed energy, and E_k is the kinetic energy.

3. Results and discussion

The main task of this study is to investigate the solid–liquid phase change and the resulting structure of silicon upon ultrafast laser irradiation. In order to explain phase change induced by an ultrafast laser pulse, the equilibrium melting temperature of crystalline silicon is first computed using the Stillinger–Weber potential function described in Refs. [27–29].

3.1. Determining the equilibrium melting temperature of crystalline silicon

A small computational domain consisting of 1296 atoms and with size of 1.63 nm × 1.63 nm × 9.78 nm (x, y, z: 3, 3, 18 unit cells and each unit cell is occupied by one silicon lattice and each silicon lattice cubic contains 8 silicon atoms) is used for computing the equilibrium melting temperature of crystalline silicon. In order to allow expansion along the z-direction, extra 18 unit cells, which are the empty space for the purpose of allowing the motions of atoms at the two sides surfaces when temperature increases, are added both above and below the target along the z-direction. The computational domain is illustrated in Fig. 1(a).

To find out the equilibrium melting temperature of crystalline silicon, equilibrium states are computed at different temperatures. Fig. 2(1–4) below show the atom structures of sample with a series of different temperatures (1780 K, 1800 K, 1850 K, 1870 K) near melting at two time 2 ps and 200 ps. It can be seen that the surface of the sample starts to melt at about 1780 K but the rest part of thin film remains as solid due to the higher surface energy of the atoms at the surface. Besides that, at 1780 K, the atom structure

Table 1
Values of parameters used in the equations.

Parameter	Value
m[a], silicon atomic mass (Kg)	$28.0855 \times 1.66 \times 10^{-27}$
k_B[b], Boltzmann's constant	1.38×10^{-23}
δ[c], laser penetration depth (m)	5.54×10^{-9}
Δt[d], time step (s)	2.0×10^{-16}
t_0, time for peak laser intensity (s)	10×10^{-12}
t_g, laser pulse width, full width at half maximum (FWHM) (s)	3×10^{-12}

[a] Reference [50].
[b] Reference [10].
[c] Reference [51].
[d] Reference [27].

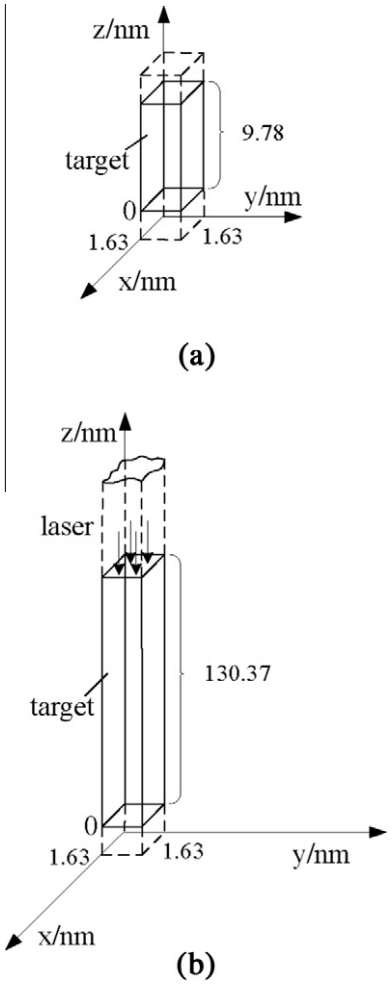

Fig. 1. Scheme of the computational domain of (a) equilibrium state system and (b) laser heating system.

does not change whereas for all others the structures keep evolving until the material is completely melted. Therefore, the states above 1780 K are not equilibrium states. For studying the laser-induced phase change as discussed below, we take 1780 K as the equilibrium melting temperature determined by the Stillinger–Weber potential employed in this study.

Compared with the experimental melting point of solid silicon, 1683 K [36], the melting temperature calculated in our work 1780 K is about 100 K higher. This difference can be caused by a number of reasons. As we know [37], the uniaxial expansion and associated anisotropic lattice distortions can affect the melting temperature. It has been shown that the anisotropic deformation reduces the lattice stability against the initiation of melting. Similarly, a uniaxial expansion of the system and anisotropic distortions of the lattice caused by increasing temperature will have similar effect as that in Ref. [37] on the melting temperature [38], which leads to a higher equilibrium melting temperature of 1780 K in our study. Furthermore, the different method or different boundary conditions used in our calculations also contribute the difference in our melting temperature compared with the literature values [27,39,33,36,40].

3.2. Temperature evolution and phase and structural change of crystalline silicon irradiated by an ultrafast laser pulse

A sample, consisting of 17,280 atoms and with a size of 1.63 nm × 1.63 nm × 130.37 nm (x, y, z: 3, 3, 240 unit cells and

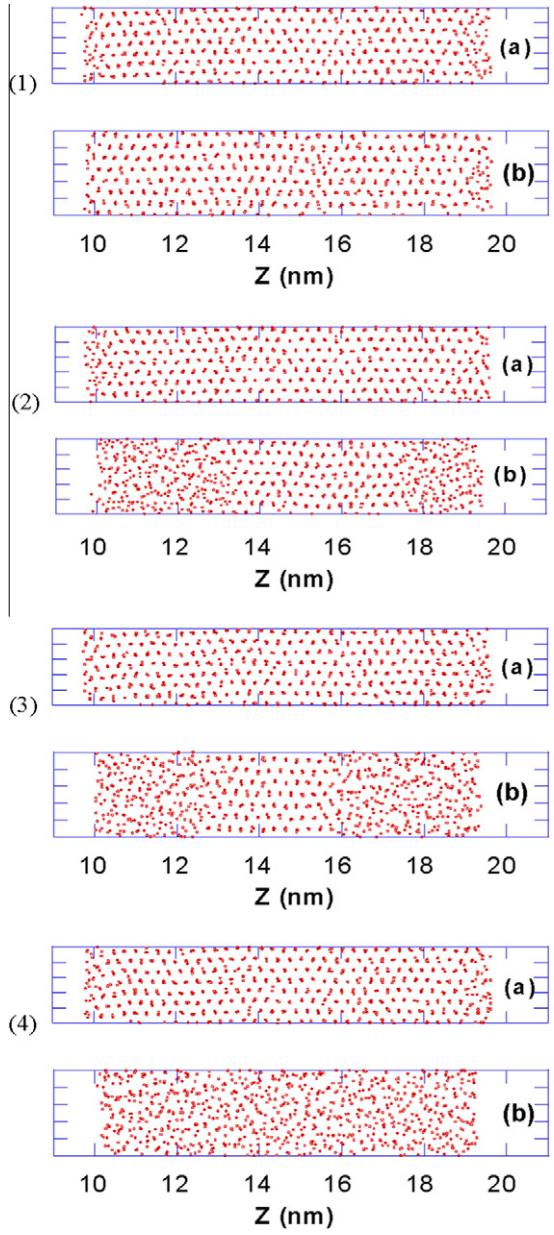

Fig. 2. Atomic structures at different temperatures of (1) 1780 K (a)1780 K – 2 ps, (b)1780 K – 200 ps, (2) 1800 K (a)1800 K – 2 ps, (b)1800 K – 200 ps, (3) 1850 K (a)1850 K – 2 ps, (b)1850 K – 200 ps, (4) 1870 K (a)1870 K – 2 ps, (b)1870 K – 200 ps.

each unit cell is occupied by one silicon lattice and each silicon lattice cubic contains 8 silicon atoms), is used for the study of ultrafast laser heating. For the purpose of allowing the motions of atoms at the surface, extra 480 empty unit cells and 120 empty unit cells, which are the empty space for the purpose of allowing the motions of atoms at the two sides surfaces when laser heating starts, are added to top and bottom of the target along the *z*-direction, respectively. The computational domain is shown in Fig. 1(b).

Figs. 3 and 4 show the temperature distribution in silicon when the target surface is irradiated by laser pulses with fluences of 60 J/m^2 and 90 J/m^2, respectively. It is seen that there is a rapid temperature rise at the surface around the time when the laser intensity reaches its peak value at 14 ps. As time progresses, the absorbed energy is transferred to other atoms beneath the surface through inter-atomic interactions. At the end of the computation period, 200 ps, the target reaches a uniform temperature.

The peak temperatures obtained in Figs. 3 and 4 have exceeded the equilibrium melting temperature calculated in Section 3.1. In order to illustrate the structural evolution, the positions of atoms near the surface where the phase change occurs are plotted in Fig. 5 for the laser fluence of 60 J/m^2. As shown in Fig. 5(b), the atomic structure is kept as that of the equilibrium state till about 14 ps when the temperature reaches 2066 K, above the melting point. The laser heating process continues till 20 ps, about the end of the laser pulse. The melt depth reaches a maximum depth of 2.68 nm, and then resolidification starts. It is noted that after the melted region is completed solidified, some of the materials near the surface remains as amorphous as shown in Fig. 5(i). At 200 ps, the temperature of target tends to be uniform at 485 K as shown in Fig. 3(b). Therefore, the computational domain is completed solidified. More analysis of the resolidification process will be discussed below. The thickness of this amorphous layer is about 2.05 nm (the top surface is located at 195.55 nm), less than the maximum melt depth of 2.68 nm. This will be discussed later.

Similar structural changes are observed when the laser fluence is 90 J/m^2, except that a higher peak temperature of 5121 K (20 ps) is obtained. The maximum melt depth is 5.60 nm, and the resulting amorphous layer after resolidification is 4.11 nm.

3.3. Interface kinetics and the resulting silicon structure

The results from the MD calculations offer an opportunity to investigate the interface kinetics, i.e., interface superheating and undercooling temperature in the phase change process induced by an ultrafast laser pulse, and its effect on the resulting structures.

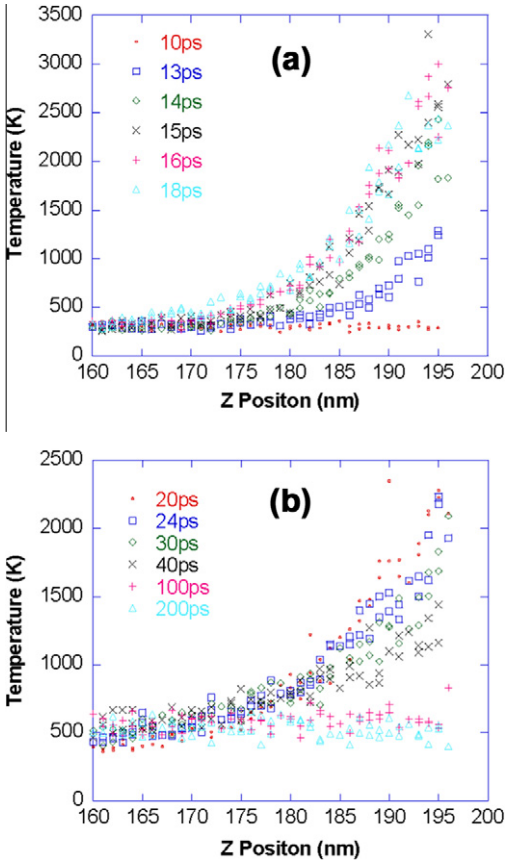

Fig. 3. Temperature evolution for a laser fluence of 60 J/m^2 (a) 10–18 ps, (b) 20–200 ps.

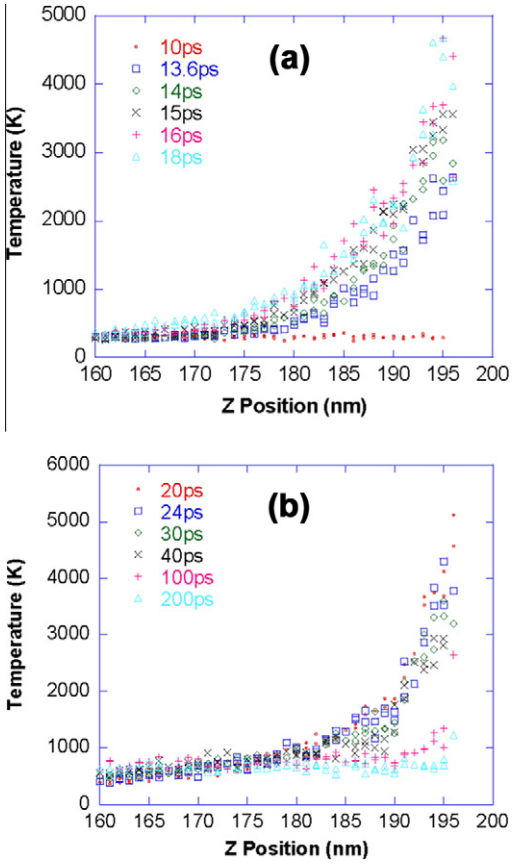

Fig. 4. Temperature evolution for a laser fluence of 90 J/m^2 (a) 10–18 ps, (b) 20–200 ps.

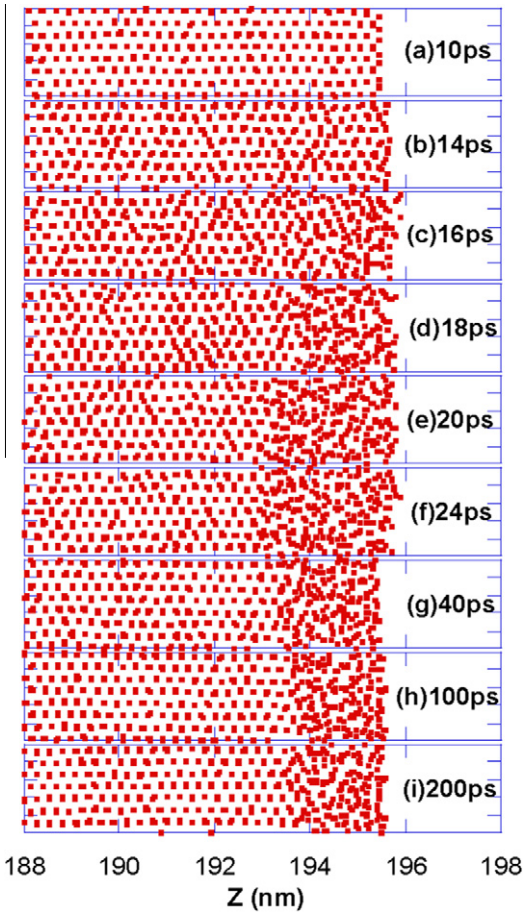

Fig. 5. Structural change at laser fluence of 60 J/m^2 at times of (a) 10 ps, (b) 14 ps, (c) 16 ps, (d) 18 ps, (e) 20 ps,(f) 24 ps, (g) 40 ps, (h) 100 ps, and (i) 200 ps. The average temperatures of the top 5 atomic layers are (a) 300 K, (b) 2065 K, (c) 2692 K, (d) 2286 K, (e) 2107 k, (f) 1928 K, (g) 1234 K, (h) 614 K, (i) 485 K.

According to the interface kinetic theory of solid–liquid phase change [41], when the melt-solid interface moves with a finite velocity, the temperature at the interface is expected to deviate from the equilibrium melting temperature. The interfacial superheating/undercooling temperature at the interface: $\Delta T = T_{eq} - T_{int}$, is related to the interface velocity $V_{int}(T_{int})$ as [42,43]. Where T_{eq} is the equilibrium melting temperature, T_{int} and V_{int} are the interface temperature and velocity respectively. When ΔT is small, V_{int}, and ΔT at the interface can be approximated by a linear relation:

$$\Delta T = C_1 V_{int}(T_{int}) \tag{3}$$

The constant C_1 is material dependent. ΔT and V_{int} can be obtained by analyzing the MD results, therefore, allowing the determination of the value of C_1.

Relatively little work being done to determine the interface velocity-superheating/undercooling function even for single-component materials because of the technical difficulties in measuring the interface temperature during rapid resolidification, however, in order to analyze interface kinetics, the interface location and the interface temperature need to be determined. The interface location is determined by analyzing the atomic structure at a given time. For example, Fig. 5(c) shows the atom distribution near the surface for the laser fluence of 60 J/m^2 at 16 ps. It can be seen that the melting interface lies at about 194.5 nm (1.05 nm from the surface) which is the transition of crystal and liquid state silicon. The temperatures of the interfaces at the crystal–liquid and liquid-amorphous boundaries were determined by averaging the kinetic energy of the atoms in a given slice. Therefore, the average temperature of atoms between 194 nm and 195 nm is 2246 K, which is taken as the interface temperature. Similarly, the interface location and the corresponding interface temperature are obtained for other time steps during melting process, which are all higher than the equilibrium melting temperature of 1780 K.

However, it is not possible to determine the interface location by inspecting the atomic structure during resolidification process, since the material can remain amorphous after resolidification, as shown in Fig. 5(i). In order to distinguish the crystalline, liquid, and amorphous silicon during and after resolidification process, the radial distribution function (RDF) [16,34] is used. RDF [44–46], with the ability to characterize the in-plane structure, is becoming widely used in MD simulation to distinguish phases of a material. It is a ratio of the number of atoms at a distance r from a given atom compared with the average atomic number density in an ideal crystal. RDFs for the three phases of silicon are shown in Fig. 6, which are calculated from three different positions at z directions at 30 ps, and each location is calculated using 216 atoms. The RDF of c-Si has periodic peaks which reflect the crystalline structure. The long-range periodicity is the main characteristic for ideal c-Si. Both l-Si and a-Si have similar long-range disorders – no peaks for larger r. l-Si and a-Si are distinguished by small differences in the shorter range. The RDF of a-Si has higher first and second peaks than that of l-Si, and l-Si possesses the smoothest RDF curve, which means more short-range disorders in l-Si than that in a-Si. The difference in the RDF allows for the determination of the location of interface at each time step during the resolidification process. Compared with the existing methods of solid–liquid interface location determination, such as, observing

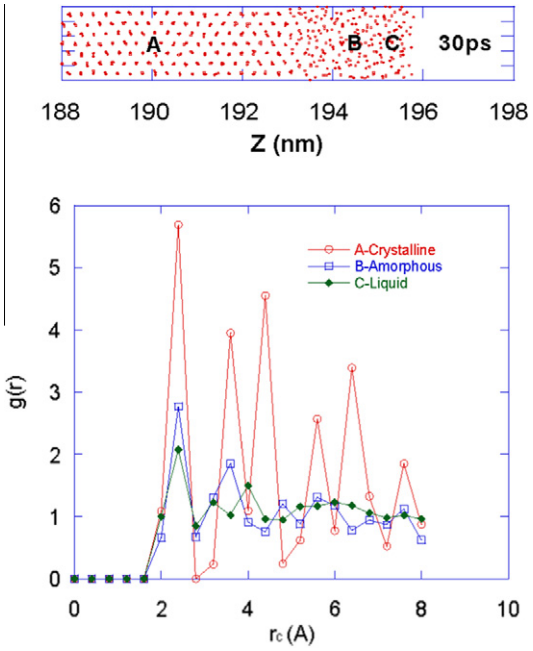

Fig. 6. The radial distribution functions of three phases of silicon with a laser fluence of 60 J/m^2. A. Crystalline RDF [*z*: 189.8–190.2 nm]; B. Amorphous RDF [*z*: 194.4–194.8 nm]; C. Liquid RDF [*z*: 194.8–195.2 nm].

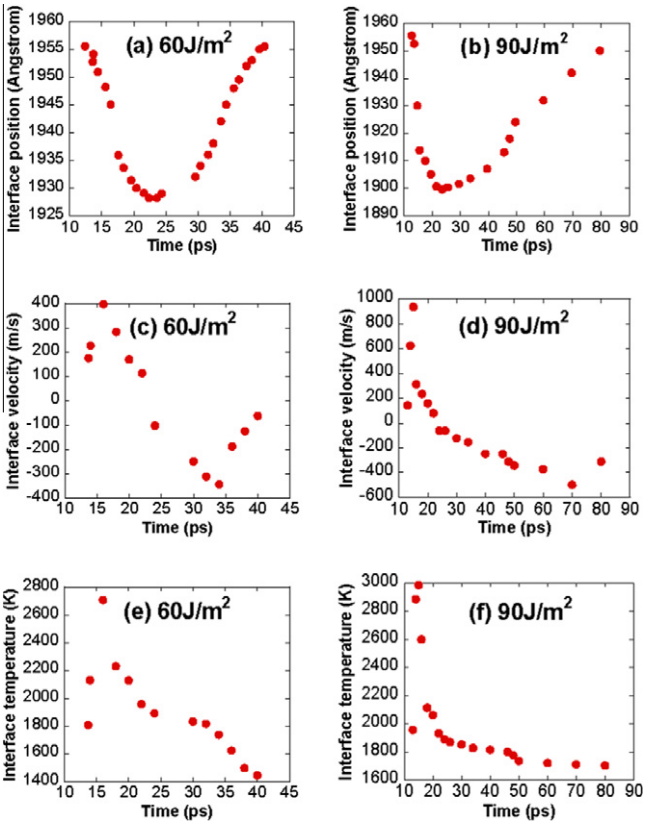

Fig. 7. The solid–liquid interface location, velocity, and temperature as a function of time at a laser fluence of (a), (c), (e) 60 J/m^2, and (b), (d), (f) 90 J/m^2.

the diffusion coefficients (*via* mean-square displacement data), the three-body potential energy [18], and the fraction of solid atoms in each layer [19,20]; or determining the order parameter of each atomic slice (two-atomic-layers thick) and classifying a slice as crystallike, liquidlike, or amorphouslike, [21], the RDF can give a reasonable identification for the solid–liquid interface location and is also a novelty proposed in this study compared with its rare application for this purpose in the past.

Fig. 7(a) and (b) shows the solid–liquid interface locations during melting and resolidification processes at the laser fluences of 60 J/m^2 and 90 J/m^2, respectively. The interface velocities are taken as the derivative of the interface locations, and are plotted in Fig. 7(c) and (d). It is seen that the maximal melting depth is reached rapidly at 23 ps and 23.6 ps for the two fluences, followed by a relatively slower resolidification process. The interface temperatures are plotted in Fig. 7(e) and (f). It is seen that for both 60 J/m^2 and 90 J/m^2, the interface velocity and interface temperature have similar trends, indicating that the interface kinetics – the interface velocity – temperature relation follows roughly a linear relation expressed by Eq. (3). Some deviations, particularly near the end of the resolidification process (the velocity slows down toward the end of the resolidification process while the temperature continues to decrease) are probably due to the uncertainties in determining the interface location accurately using the RDF method. It is also possible that the lower surface energy of solid slows down the resolidification process when the interface approaches the surface, which is not considered in the kinetic theory described by Eq. (3). Please note here we did not discuss the possible impact from the reflection of a pressure wave on the determination of temperature, which can be eliminated through applying the nonreflective boundary condition to the bottom of the sample [34,35]. The reason is because we have used the structure change and RDFs to track liquid–solid (crystal and amorphous) interfaces and the effect from the reflection of a pressure wave has been implicitly included.

As seen in Fig. 5, the maximum melt depth is larger than the thickness of the final amorphous layer. Therefore, resolidification of liquid silicon first forms a layer of crystalline silicon, and then amorphous silicon. This phenomenon can be correlated with the MD results that the resolidification process is first a slower process when it starts at the maximum melt depth and near the equilibrium melting temperature, and then accelerated as the temperature is reduced. The final microstructures and the computed resolidification front velocity and temperature suggest a strong correlation between the resolidification velocity and the resulting microstructure, that a larger resolidification velocity results in an amorphous state, and a smaller velocity results in a crystalline state. And also the crystallization occurs in a shorter time with a slower velocity and leads to thinner crystal silicon layer, while the amorphization continues a longer time at faster velocity and results in a thicker amorphous silicon layer.

Furthermore, the quantitative relationship between final state of the material, amorphous and crystal, and the velocity of resolidification interface has also been explored. The average velocity for forming crystalline silicon is estimated to be about 74 m/s and 67 m/s for 60 J/m^2 and 90 J/m^2, respectively, and the average velocity for forming amorphous silicon is 230 m/s and 120 m/s for 60 J/m^2 and 90 J/m^2, respectively. However, compared with experimental and simulation results of maximum crystallization velocity for Si in some literatures [17,47–49], the results from our study are very rough estimates as there are uncertainties to determine the boundaries of the states.

4. Conclusions

In this work, molecular dynamics simulations were carried out to explore interactions between ultrafast laser pulse and crystalline silicon. Solid–liquid phase change and the resulting structural change were evaluated. It was found that the temperature at the

solid–liquid melt front exceeded the equilibrium melting temperature by several hundred degrees during melting, and was lower than the equilibrium temperature by several hundred degrees during resolidification. This interface superheating and undercooling temperatures were correlated with the interface velocity, and were consistence with the solid–liquid interface kinetic theory. Based on the ability to characterize phases of a material, the RDF was attempted to be used to determine the interface location of crystalline-liquid and liquid-amorphous silicon during resolidification and gives a reasonable identification. The resolidification process first produced thinner crystalline silicon layer due to the relatively low resolidification speed in a shorter time, and then thicker amorphous silicon layer as the resolidification speed increases within a longer time. Divergence between our results and previous experimental and simulation results [17,47–49] through the quantitative comparison reflects the results from our study are very rough estimates as there are uncertainties to determine the boundaries of the states.

Acknowledgements

The authors thank the partial support by the Panasonic Boston Laboratory of Panasonic R&D Company of America. One of the authors (C.Y.) is thankful for the fellowship provided by the Chinese Scholarship Council.

References

[1] W. Heywang, K.H. Zaininger, Silicon: Evolution and Future of a Technology, in: P. Siffert, E.F. Krimmel (Eds.), Silicon: The Semiconductor Material, Springer Verlag, 2004.
[2] B.C. Stuart, M.D. Feit, A.M. Rubenchik, B.W. Shore, M.D. Perry, Laser-induced damage in dielectrics with nanosecond to subpicosecond pulses, Phys. Rev. Lett. 74 (12) (1995) 2248–2251.
[3] S. Nolte, C. Momma, H. Jacobs, A. Tünnermann, B.N. Chichkov, B. Wellegehausen, H. Welling, Ablation of metals by ultrashort laser pulses, J. Opt. Soc. Am. B 14 (10) (1997) 2716–2722.
[4] S. Preuss, A. Demchuk, M. Stuke, Sub-picosecond UV laser ablation of metals, Appl. Phys. A 61 (1995) 33–37.
[5] P.L. Liu, R. Yen, N. Bloembergen, R.T. Hodgson, Picosecond laser-induced melting and resolidification morphology on Si, Appl. Phys. Lett. 34 (1979) 864–866.
[6] C.V. Shank, R. Yen, C. Hirlimann, Time-resolved reflectivity measurements of femtosecond-optical-pulse-induced phase transitions in silicon, Phys. Rev. Lett. 50 (1983) 454–457.
[7] M.C. Downer, R.L. Fork, C.V. Shank, Femtosecond imaging of melting and evaporation at a photoexcited silicon surface, J. Opt. Soc. Am. B 2 (4) (1985) 595.
[8] T.Y. Choi, C.P. Grigoropoulos, Plasma and ablation dynamics in ultrafast laser processing of crystalline silicon, J. Appl. Phys. 92 (9) (2002) 4918–4925.
[9] X. Xu, C. Cheng, I.H. Chowdhury, Molecular dynamics study of phase change mechanisms during femtosecond laser ablation, J. Heat Transfer 126 (2004) 727–734.
[10] X. Wang, X. Xu, Molecular dynamics simulation of thermal and thermomechanical phenomena in picosecond laser material interaction, Int. J. Heat Mass Transfer 46 (2002) 45–53.
[11] L.V. Zhigilei, B.J. Garrison, Microscopic mechanisms of laser ablation of organic solids in the thermal and stress confinement irradiation regimes, J. Appl. Phys. 88 (3) (2000) 1281–1298.
[12] L.V. Zhigilei, Dynamics of the plume formation and parameters of the ejected clusters in short-pulse laser ablation, Appl. Phys. A 76 (2003) 339–350.
[13] T. Ikamoto, E. Ohmura, T. Sanno, Y. Morishige, I. Miyamoto, Analytical study on metal microstructures using femtosecond laser, Appl. Phys. A 81 (2005) 639–643.
[14] R. Fedosejevs, S.E. Kirkwood, R. Holenstein, N. Young, Y.Y. Tsui, Femtosecond interaction processes near threshold: damage and ablation, Proc. SPIE 6403 (2007) 640302.1–640302.10.
[15] R.F.W. Herrmann, J. Gerlach, E.E.B. Campbell, Molecular dynamics simulation of laser ablation of silicon, Nucl. Instrum. Methods Phys. Res., Sect. B 122 (1997) 401–404.
[16] L. Tian, X. Wang, Pulsed laser-induced rapid surface cooling and amorphization, Jpn. J. Appl. Phys. 47 (2008) 8113–8119.
[17] Q.M. Yu, M.O. Thompson, P. Clancy, Solidification kinetics in SiGe alloys, Phys. Rev. B 53 (1996) 8386–8397.
[18] M.J. Uttormark, S.J. Cook, M.O. Thompson, P. Clancy, Dissolution dynamics of sub-critical clusters in liquid silicon, Mater. Res. Soc. Symp. Proc. 205 (1992) 417–422.
[19] Q.M. Yu, P. Clancy, Molecular dynamics simulation of crystal growth in $Si_{1-x}Ge_x$/Si (100) heterostructures, J. Cryst. Growth 149 (1995) 45–58.
[20] L.G. Wang, P. Clancy, M.O. Thompson, C.S. Murthy, Thermodynamic and kinetic studies of laser thermal processing of heavily boron-doped amorphous silicon using molecular dynamics, J. Appl. Phys. 92 (2002) 2412–2419.
[21] E.J. Albenze, M.O. Thompson, P. Clancy, Atomistic computer simulation of explosive crystallization in pure silicon and germanium, Phys. Rev. B 70 (2004) 094110.1–094110.10.
[22] J.A. Yater, Ph.D. Thesis, Cornell University, Ithaca, New York, 1992.
[23] A. Borowiec, M. Mackenzie, G.C. Weatherly, H.K. Haugen, Transmission and scanning electron microscopy studies of single femtosecond laser-pulse ablation of silicon, Appl. Phys. A 76 (2003) 201–207.
[24] J. Bonse, K.-W. Brzezinka, A.J. Meixner, Modifying single-crystalline silicon by femtosecond laser pulses: an analysis by micro Raman spectroscopy, scanning laser microscopy and atomic force microscopy, Appl. Surf. Sci. 221 (2004) 215–230.
[25] M.S. Amer, M.A. El-Ashry, L.R. Dosser, K.E. Hix, J.F. Maguire, B. Irwin, Femtosecond versus nanosecond laser machining: comparison of induced stresses and structural changes in silicon wafers, Appl. Surf. Sci. 242 (2005) 162–167.
[26] X. Wang, X. Xu, Molecular dynamics simulation of heat transfer and phase change during laser material interaction, J. Heat Transfer 124 (2002) 265–274.
[27] F.H. Stillinger, T.A. Weber, Computer simulation of local order in condensed phases of silicon, Phys. Rev. B 31 (1985) 5262–5271.
[28] S.J. Cook, P. Clancy, Comparison of semi-empirical potential functions for silicon and germanium, Phys. Rev. B 47 (1993) 7686–7699.
[29] D.C. Rapaport, The Art of Molecular Dynamics Simulation, second ed., Cambridge University Press, 1995.
[30] C.F. Richardson, P. Clancy, Picosecond laser processing of copper and gold: a computer simulation study, Mol. Simulat. 7 (1991) 335.
[31] S.J. Cook, P. Clancy, Impurity segregation in LennardJones A/AB heterostructures. I. The effect of lattice strain, J. Chem. Phys. 99 (1993) 2175–2191.
[32] S.J. Cook, P. Clancy, Impurity segregation in LennardJones A/AB heterostructures. II. The effect of impurity size, J. Chem. Phys. 99 (1993) 2192–2201.
[33] H. Balamane, T. Halicioglu, W.A. Tiller, Comparative study of silicon empirical interatomic potentials, Phys. Rev. B 46 (1992) 2250–2279.
[34] C. Cheng, X. Xu, Molecular dynamics calculation of critical point of nickel, Int. J. Thermophys. 28 (2007) 9–19.
[35] C. Cheng, X. Xu, Molecular dynamics simulation of ultrafast laser ablation of fused silica, J. Phys. 59 (2007) 100–104.
[36] J.Q. Broughton, X.P. Li, Phase diagram of silicon by molecular dynamics, Phys. Rev. B 35 (1987) 9120–9127.
[37] D.S. Ivanov, L.V. Zhigilei, Effect of pressure relaxation on the mechanisms of short-pulse laser melting, Phys. Rev. Lett. 91 (2003) 105701.1–105701.4.
[38] D.S. Ivanov, L.V. Zhigilei, Combined atomistic-continuum model for simulation of laser interaction with metals: application in the calculation of melting thresholds in Ni targets of varying thickness, Appl. Phys. A 79 (2004) 977–981.
[39] B.J. Thijsse, Relationship between the modified embedded-atom method and Stillinger–Weber potentials in calculating the structure of silicon, Phys. Rev. B 65 (2002) 195207.1–195207.5.
[40] J.-P. Hansen, L. Verlet, Phase transitions of the Lennard-Jones system, Physiol. Rev. 184 (1969) 151–161.
[41] K.A. Jackson, in: R. Ueda, J.B. Mullin (Eds.), Crystal Growth and Characterization, North-Holland, Amsterdam, 1975, p. 21.
[42] X. Xu, C.P. Grigoropoulos, R.E. Russo, Heat transfer in excimer laser melting of thin polysilicon layers, J. Heat Transfer 117 (1995) 708–715.
[43] X. Xu, G. Chen, K.H. Song, Experimental and numerical investigation of heat transfer and phase change phenomena during excimer laser interaction with nickel, Int. J. Heat Mass Transfer 42 (1999) 1371–1382.
[44] M.P. Allen, D.J. Tildesley, Computer Simulation of Liquids, Clarendon Press, Oxford, 1987.
[45] X. Wang, Thermal and Thermomechanical Phenomena in Laser Material Interaction, Ph.D. thesis, Purdue University, West Lafayette, Indiana (2001).
[46] D.K. Chokappa, S.J. Cook, P. Clancy, Nonequilibrium simulation method for the study of directed thermal processing, Phys. Rev. B 39 (1989) 10075–10087.
[47] M.O. Thompson, J.W. Mayer, A.G. Cullis, H.C. Webber, N.G. Chew, J.M. Poate, D.C. Jacobson, Silicon melt, regrowth, and amorphization velocities during pulsed laser irradiation, Phys. Rev. Lett. 50 (1983) 896–899.
[48] P.A. Stolk, A. Polman, W.C. Sinke, Experimental test of theories for heterogeneous freezing kinetics in silicon, Phys. Rev. B 47 (1993) 5.
[49] A. Polman, P.A. Stolk, D.J.W. Mous, W.C. Sinke, C.W.T. Bulle-Lieuwma, D.E.W. Vandenhoudt, Pulsed-laser crystallization of amorphous silicon layers buried in a crystalline matrix, J. Appl. Phys. 67 (1990) 4024.
[50] M.E. Wieser, Atomic weights of the elements 2005 (IUPAC TECHNICAL REPORT), Pure Appl. Chem. 78 (2006) 2051–2066.
[51] J. Meijer, Laser beam machining (LBM), state of the art and new opportunities, J. Mater. Process. Tech. 149 (2004) 2–17.